NATIONAL AERONAUTICS AND SPACE ADMINISTRATION

Technical Report 32-1035

A Treatise on the Surveyor Lunar Landing Dynamics and an Evaluation of Pertinent Telemetry Data Returned by Surveyor I

F. Sperling
J. Garba

JET PROPULSION LABORATORY
CALIFORNIA INSTITUTE OF TECHNOLOGY
PASADENA, CALIFORNIA

August 15, 1967

NATIONAL AERONAUTICS AND SPACE ADMINISTRATION

Technical Report 32-1035

A Treatise on the Surveyor Lunar Landing Dynamics and an Evaluation of Pertinent Telemetry Data Returned by Surveyor I

F. Sperling
J. Garba

Approved by:

M. E. Alper

M. E. Alper, *Manager*
Applied Mechanics Section

JET PROPULSION LABORATORY
CALIFORNIA INSTITUTE OF TECHNOLOGY
PASADENA, CALIFORNIA

August 15, 1967

TECHNICAL REPORT 32-1035

Prepared Under Contract No. NAS 7-100
National Aeronautics & Space Administration

Acknowledgment

This report includes direct or indirect contributions by a large number of individuals, not only at the Jet Propulsion Laboratory but also at the Hughes Aircraft Company, the prime *Surveyor* contractor, as well as many other industrial subcontractors. The authors express their thanks and appreciation, generally, to everyone involved. However, specific acknowledgment should be extended to Ralph E. Deitrick and Reginald H. Jones, of the Hughes Aircraft Company, who were instrumental in conceiving and carrying through the *Surveyor* landing gear design and implementation, and to Robert G. Alderson and David A. Wells, of the Bendix Products Aerospace Division, for providing the landing simulation program, without which the subject data evaluation and lunar soil study would not have been possible.

Contents

Contents (contd)

Tables

Figures

Abstract

The lunar landing of a *Surveyor* spacecraft is investigated from the viewpoint of landing dynamics, which includes the dynamic behaviour of the spacecraft as well as that of the lunar surface material during the landing process. A description is given of the landing gear design, the final descent and landing sequence, and the analytical and experimental qualification programs conducted. The evaluation of landing telemetry data concentrates on the *Surveyor I* mission, although preliminary results of *Surveyor III* are briefly discussed. In a parametric landing simulation study, the best agreement between analytical and flight data was found to be associated with a dynamic soil model having a bearing strength between 0 and 2 psi at the surface, and between 6 and 8 psi at a depth of 2 in., when penetrated by a *Surveyor* footpad.

A Treatise on the *Surveyor* Lunar Landing Dynamics and an Evaluation of Pertinent Telemetry Data Returned by *Surveyor I*

I. Introduction

At 06:17:34 GMT, June 2, 1966, the spacecraft *Surveyor I* performed a controlled soft landing on the surface of the Moon in a location 43.35 deg west and 2.58 deg south. This report presents a description of the *Surveyor* landing from a dynamic point of view. An assessment of the dynamic performance of the spacecraft during the final descent and landing phase is given, and an attempt is made to estimate the dynamic behavior of the surface material as indicated by the engineering telemetry and TV data.

The *Surveyor I* mission was the first in a series of *Surveyor* engineering missions; i.e., its main objective was to demonstrate the feasibility of the radar-controlled soft landing technique. There are two more general objectives of the *Surveyor* program as defined by NASA: to obtain data of the lunar surface in support of the *Apollo* Program, and to increase the scientific knowledge of the Moon. The upcoming scientific *Surveyor* missions will be specifically equipped to accomplish these goals. However, some conclusions regarding these objectives can be drawn from data obtained during the *Surveyor I* landing.

The second *Surveyor* mission (Mission B) was conducted in February 1967. Because of a failure in the vernier propulsion system during midcourse correction maneuver, the spacecraft went into a tumbling motion from which it could not be recovered.

Surveyor Mission C was performed in April 1967, while this report was being reviewed for release. A soft landing of *Surveyor III* on the lunar surface was accomplished at 00:04:18 GMT, April 20, 1967, in a location 23.34 deg west and 2.94 deg south. Except for the addition of the Surface Sampler Experiment to *Surveyor III*, there was very little difference between *Surveyor I* and *III* in regard to the spacecraft, as well as the planned mission profile. The nominal lunar descent and landing profile was identical for both spacecraft; however, in Mission C, it was not followed according to plan in all

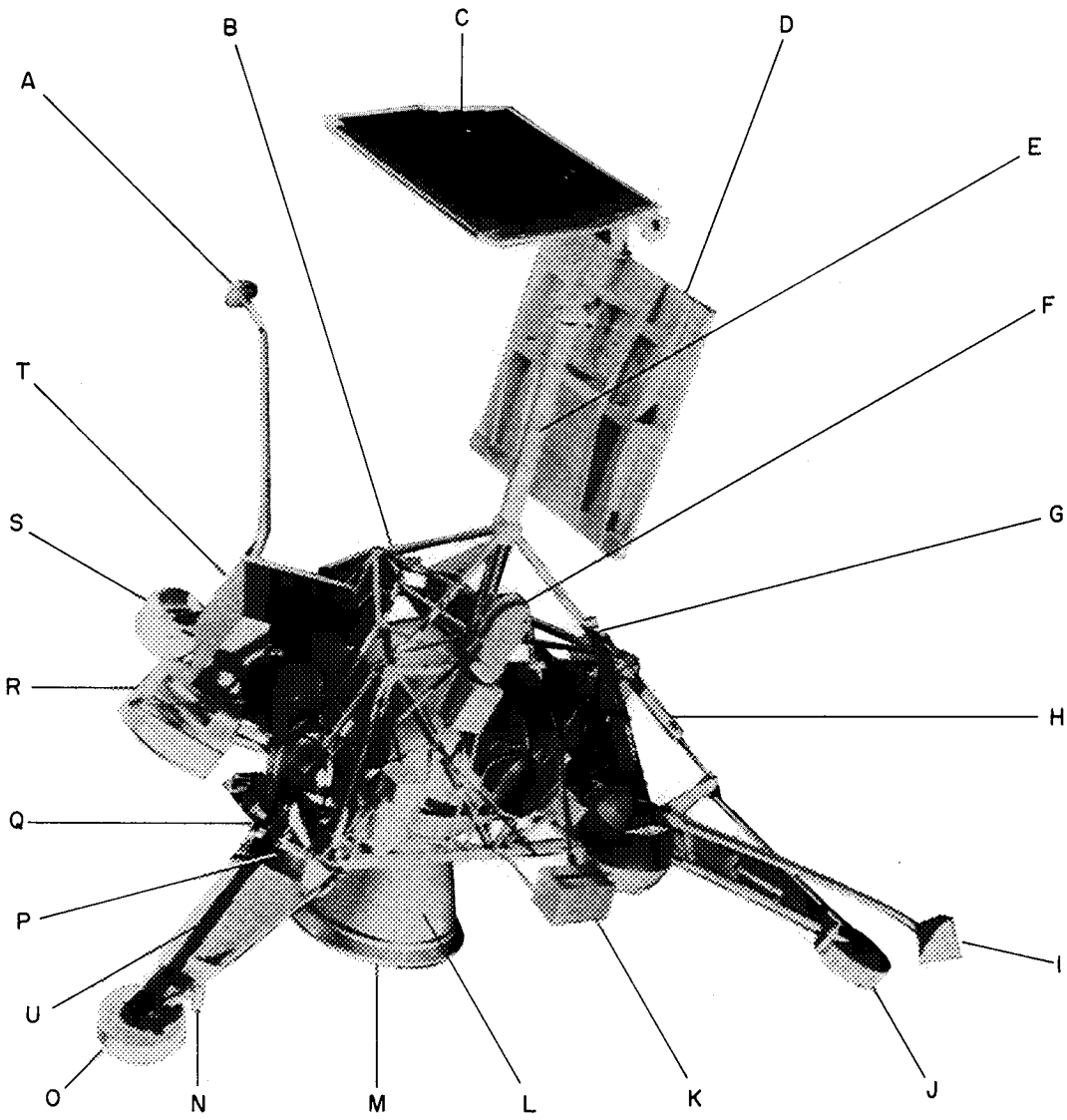

A OMNIDIRECTIONAL ANTENNA A
B SPACEFRAME
C SOLAR PANEL
D PLANAR ARRAY ANTENNA
E MAST
F SURVEY TELEVISION CAMERA
G FLIGHT CONTROL SENSORS
H LANDING LEG LOCK STRUT (3)
I OMNIDIRECTIONAL ANTENNA B
J LANDING GEAR LEG 3
K AUXILIARY BATTERY
L MAIN RETROROCKET ENGINE
M AMR ANTENNA (MOUNTED IN NOZZLE)
N COLD GAS ATTITUDE JET (3)
O LANDING GEAR LEG 2
P CRUSHABLE BLOCK (3)
Q VERNIER ENGINE (3)
R RADVS ANTENNA (2)
S LANDING GEAR LEG 1
T THERMALLY CONTROLLED COMPARTMENT (2)
U SHOCK ABSORBER (3)

Fig. 1. *Surveyor I* spacecraft configuration

aspects. Engine cutoff, nominally occurring automatically at an altitude of approximately 13 ft above the lunar surface, was not executed at this time. With the engines thrusting, the effective weight of the spacecraft was reduced by approximately 90%, which, in conjunction with the landing gear elasticity, caused a high springback after the first surface contact. A second touchdown occurred approximately 24 seconds after the first, again followed by a considerable rebound. A ground command to terminate engine thrusting was sent and executed 35.8 sec after first ground contact. One-half second later, the third and final touchdown was registered, followed by a very slight rebound and an elastic ringout, very similar to what was observed in the *Surveyor I* landing. As a consequence of the above-mentioned anomaly, the vertical touchdown velocity is estimated to have been below 5 ft/s in all three ground encounters, resulting in shock absorber peak forces of approximately half the *Surveyor I* values. Because of this, the *Surveyor III* data are not as suitable for an attempt to estimate lunar surface mechanical properties, as described in Section VII of this report, in conjunction with the data from *Surveyor I*. However, a preliminary evaluation of the *Surveyor III* data has resulted in bearing strength values which agree well with the conclusions reached in the *Surveyor I* study, as presented below.

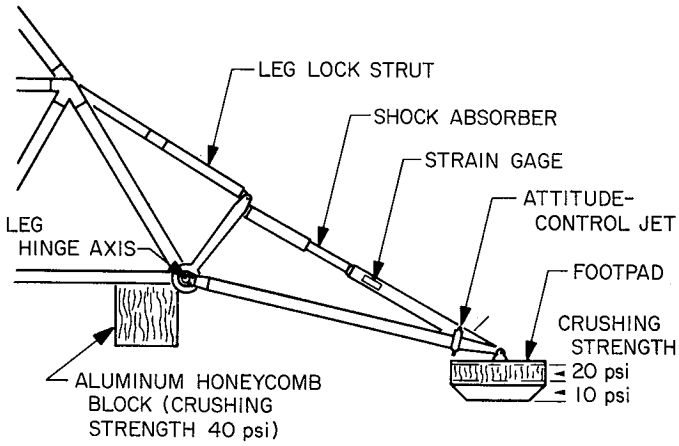

Fig. 2. *Surveyor I* landing gear in extended position (schematic)

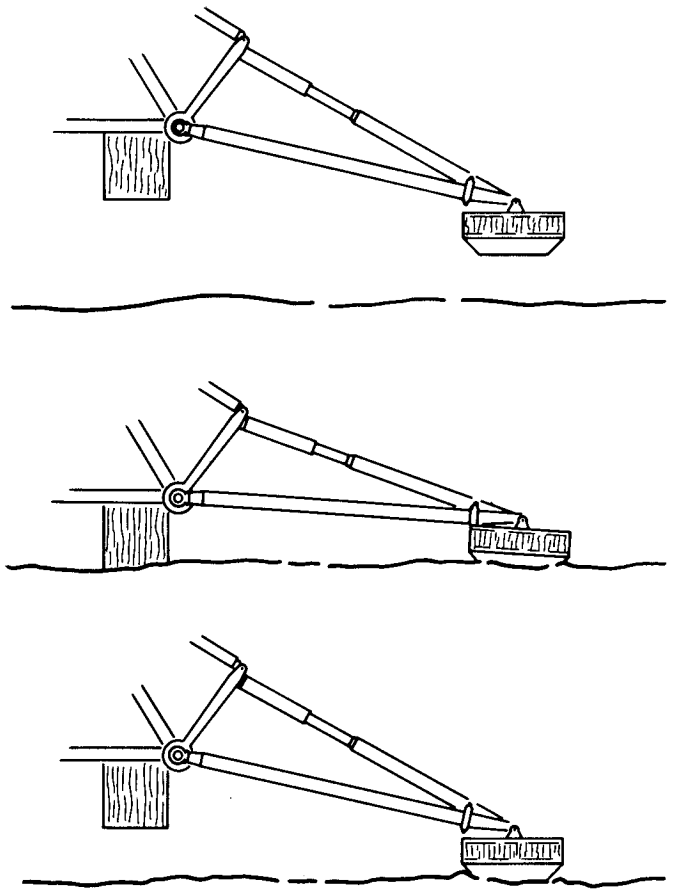

Fig. 3. *Surveyor I* landing gear articulation sequence during landing (schematic)

II. System Description

A. Spacecraft Landing System

The spacecraft structure, as illustrated by the model shown in Fig. 1, consists basically of a frame in the shape of a truncated three-sided pyramid surrounding the main retro rocket, three inverted tripod landing legs and a mast supporting the high-gain antenna and solar panel.

The landing legs are folded in during launch. They extend shortly after shroud jettison to a position schematically shown in Fig. 2. While extending, the legs rotate out about their hinge axes until the lock struts fully extend and lock. The motion during landing, as illustrated in Fig. 3, is again a rotation about the hinge axis during which the shock absorbers compress, dissipating most of the spacecraft's residual kinetic energy. Finally, the shock absorbers re-extend, returning the legs to their prelanding configurations.

The functioning of the shock absorber is that of a combined spring damper assembly. Because weight considerations prohibited the use of mechanical springs, a system was developed in which the required spring action is provided by compression of the damping fluid, as it takes place when a piston and piston rod is pushed

into a rigid cylinder entirely filled with fluid. Simultaneously, the fluid is forced through an orifice in the piston to provide a damping force which is approximately proportional to the square of the stroking velocity. During landing, this velocity is highest immediately after impact, i.e., at low stroke, decreasing rapidly with increasing stroke. To compensate for the resulting damping force vs stroke characteristic, the orifice was made to change its effective diameter during the stroking process such that the damping coefficient increases steeply with increasing stroke. The result is a damping force which is approximately constant with stroke, i.e., a maximum energy dissipation capability for a fixed peak loading is obtained. A different orifice provides high damping for the shock absorber back stroke.

A secondary energy dissipation device is provided in the form of three cylindrical body blocks made of crushable aluminum honeycomb and mounted under the frame near the leg attachment areas (Fig. 2). For a level landing on a rigid level surface, these blocks engage with the surface for vertical impact velocities exceeding 8 ft/s and absorb energy by crushing at a constant load.

The footpads, which are mounted at the tips of the landing legs and can each rotate about an axis parallel to the leg hinge axis, are also made of aluminum honeycomb material. They are designed to act as mechanical overload filters for the shock absorber assemblies; they also dissipate some landing energy. However, for a level landing as described above, they do not crush if the vertical landing velocity is below approximately 11.5 ft/s.

B. Lunar Descent and Landing Phase

The nominal lunar approach and terminal descent sequence, which was followed very closely by *Surveyor I*, may be described briefly as follows. Approximately 63 h after launch, the spacecraft is commanded to roll and pitch, or yaw, from its Sun/Canopus locked cruise attitude into a position in which the main retro thrust axis coincides with the velocity vector. Sixty miles above the lunar surface, a radar sensor called the altitude marking radar (AMR) (see Fig. 1) generates a signal which triggers the following automated descent sequence. First, the three engines of the vernier propulsion system are ignited. These liquid propellant engines, each of which is capable of being throttled within a thrust range from approximately 30 to 104 lb, provide stabilization during the main retro motor burn. One second later, the 10,000-lb thrust solid-propellant main retro motor is ignited and burns for approximately 43 s. This reduces the spacecraft velocity from 8,700 ft/s to 350 ft/s at approximately 26,000 ft altitude. The main retro motor case is then ejected, while the vernier propulsion system continues to stabilize the spacecraft, developing a constant resultant thrust of 90% of the lunar spacecraft weight; in other words the spacecraft is free falling in a one-tenth lunar gravity field. In the meantime, the Radar Altimeter and Doppler Velocity Sensors (RADVS) have acquired the lunar surface. About two seconds after retro motor case ejection, the RADVS system takes control of the further spacecraft descent; this system determines the spacecraft altitude and velocity relative to the lunar surface by means of four radar beams which are oriented as shown in Fig. 4. The RADVS measurements are fed into a closed-loop automatic control system which commands the three vernier thrust levels such that the spacecraft acquires and is subsequently guided along a segmented straight line approximation of the "gravity turn" trajectory. This trajectory has two properties which are highly desirable for a dynamically smooth landing. First, it

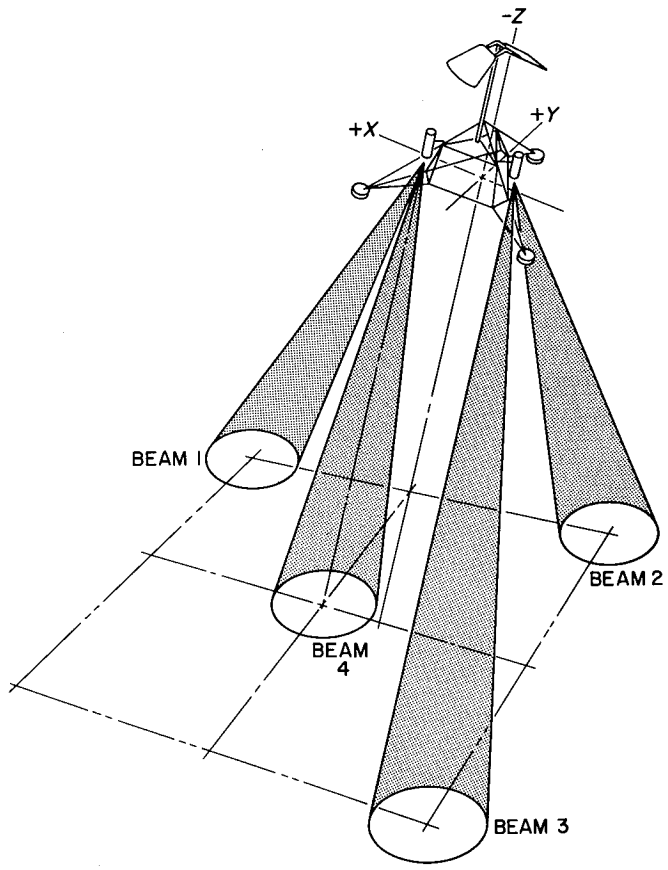

Fig. 4. RADVS beam orientation

aligns the thrust and velocity directions; i.e., the spacecraft moves along its Z-direction only (see Fig. 4 for spacecraft coordinates). Second, as the velocity approaches zero, the flight path direction (and, hence, the spacecraft Z-axis) is turned toward the lunar vertical. Because of control loop saturation, the spacecraft cannot always follow the trajectory segments precisely. However, in each segment, the actual trajectory intersects the pre-programmed line at a point called the acquisition point, from which point very close tracking ensues.

The final segment of the descent profile, together with the actual trajectory, is shown in Fig. 5. After acquisition, which occurs at approximately 80-ft altitude, the straight line is followed until the velocity reaches 10 ft/s at approximately 43-ft altitude. At this point, the RADVS system generates a signal (10-ft/s mark) which causes the RADVS control as well as the gravity turn descent profile to be abandoned and initiates the following automatic final descent sequence. The control is switched to a gyro-controlled inertial hold mode, and the vernier engines are commanded to decelerate the spacecraft rapidly to 5-ft/s vertical velocity. The spacecraft then descends with this velocity held constant until, at 13-ft altitude, a second signal is generated (13-ft mark), turning the vernier engines off. Consequently, the spacecraft falls free until the surface is encountered, increasing its

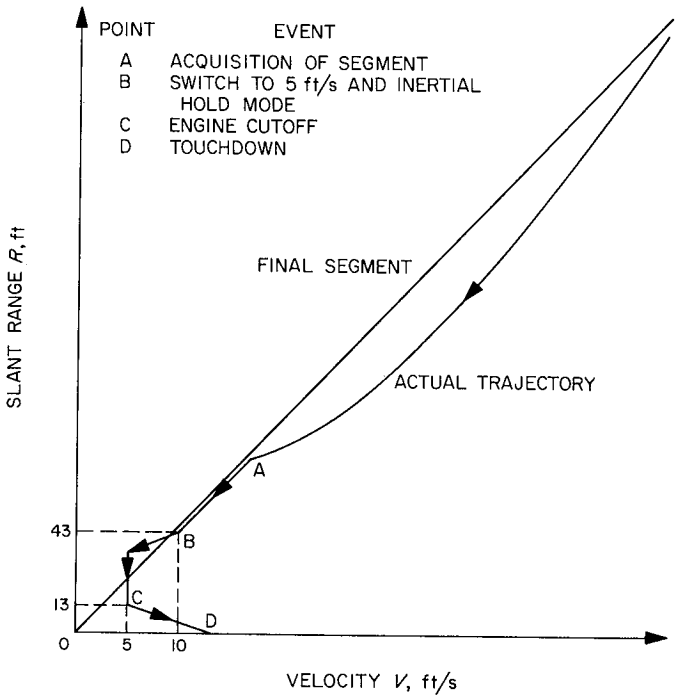

Fig. 5. Terminal descent velocity profile

vertical velocity to nominally 12.6 ft/s. Since the gravity turn descent was abandoned at 10 ft/s, the spacecraft Z-axis is not precisely vertical at this time, in which position it remains during the inertial hold mode. This introduces a horizontal velocity at touchdown because of vernier thrusting in this tilted position between the 10-ft/s and the 13-ft mark.

C. Instrumentation and Telemetry

During final descent and landing, the following measurements of interest for landing dynamics are conducted and sent to the ground station via the spacecraft telemetry link:

(1) Temperature compensated strain-gage bridges (Fig. 2) are mounted on the lower (non-telescoping) part of each shock absorber to measure the axial shock absorber force. These signals are telemetered in the form of frequency-modulated continuous analog signals.

(2) Four RADVS measurements, slant range (i.e., distance between the spacecraft and the lunar surface along the spacecraft Z-axis), and three velocity components (in spacecraft coordinates) are monitored continuously by the spacecraft. For telemetry, they are sampled by a commutator and converted into digital form. The sampling rate is two per frame for the range and the velocities along the *X*- and *Y*-axes, and eight per frame for the velocity along the Z-axis. During *Surveyor I* landing, two-frames-per-second telemetry was commanded.

(3) Three gyro readings, pitch, yaw, and roll, are also monitored continuously and sampled in the same manner as the RADVS signals at a sampling rate of two per frame.

(4) The discrete events of interest, the 10 ft/s and the 13-ft mark, are indicated by polarity changes of binary bits in a digital word which is sampled in 50-ms intervals.

III. Pre-Mission Landing Performance Assessment

A. Specified Landing Performance Requirements

The required landing performance of the *Surveyor* spacecraft is specified as follows.

The spacecraft must be capable of landing with velocities up to 20 ft/s vertically and 7 ft/s horizontally on a

rigid lunar surface, which has a slope of 15 deg or less and protuberances 10 cm or less in height, without sustaining damage that would affect its post-landing functions; however, upper three-sigma estimates for the velocities should not exceed 15 ft/s vertically and 5 ft/s horizontally. This requirement obviously includes the necessity of a stable landing, i.e., the spacecraft must land and settle in an upright position. Furthermore, the shock experienced by the spacecraft's center of gravity (cg) during landing should not exceed 30 *g* (Earth) vertically and 12 *g* (Earth) horizontally, i.e., the peak forces are not to exceed 30 and 12 times, respectively, the earth weight of the spacecraft in its landing configuration.

During the design, predictions of the above landing parameters, and others, were generated. It was then to be shown that the spacecraft was capable of performing within the predicted and/or specified regions with respect to landing stability and landing loads. In both areas, analytical simulation methods and tests of full-size test vehicles were employed.

B. Landing Stability Investigation

For an assessment of landing stability, a mathematical model was conceived simulating the kinematic and dynamic characteristics of the landing gear mounted on a rigid body with the mass and inertia properties of the *Surveyor* spaceframe and components (Refs. 1 and 2). This model was implemented into a computer-landing analysis program allowing analytical landings to be performed with any spacecraft initial conditions (attitude and velocities), an arbitrary but constant landing surface slope, and any constant surface friction coefficient. The landing surface was originally assumed to be rigid, but a later modification included the option of representing a particular type of surface softness. This program, which is also being used for data evaluation and lunar surface dynamic properties estimates, is described in detail in the computer simulation section. The landing program was first used to investigate, systematically, all possible combinations of landing parameters, i.e., spacecraft orientation and velocities at initial touchdown, lunar surface slope, and friction coefficient for two-dimensional or planar landings, i.e., landings in which the spacecraft center of mass moves in a plane containing the lunar vertical and the maximum slope direction of the assumed landing plane. This confines the landing conditions to velocities in this plane only, i.e., the spacecraft lands either uphill or downhill, or with zero horizontal velocity. Also, the spacecraft attitude is symmetrical about this plane, i.e., one leg is either leading or trailing, and if there is any initial spacecraft tilt, it is such that the spacecraft Z-axis (parallel to the mast) remains in this plane of symmetry.

As expected, the planar case most likely to be unstable was found to be a landing on a sloped surface with the horizontal velocity in the downhill direction and one leg trailing, thus minimizing the effective tipover radius. The stability boundary for this case, in connection with the maximum specified surface slope angle of 15 deg, is shown in Fig. 6, together with the velocity regions as required in the design specification and as estimated for performance (upper three-sigma estimates). The horizontal spacecraft velocity at initial touchdown, plotted along the abscissa in Fig. 6, serves as stability indicator; in other words, the horizontal velocity is varied, with all other parameters fixed, until an unstable landing is encountered. As these results show, no instability condition exists within or near the specified *Surveyor* landing velocities. Figure 6 also shows some results of the extensive experimental landing stability investigation which was conducted to supplement the

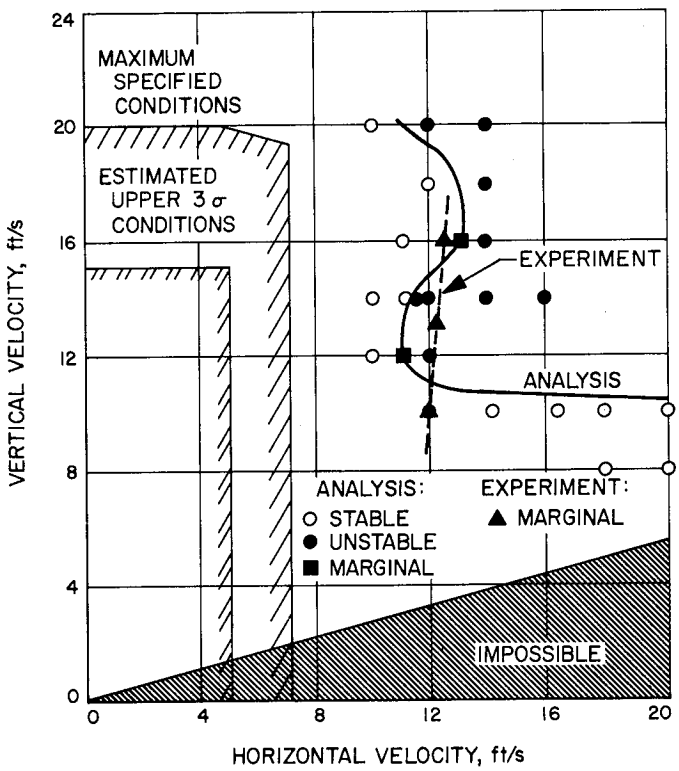

Fig. 6. Landing stability boundaries for planar downhill landings on 15-deg slope; spacecraft orientation: one leg trailing

analysis (Ref. 1). A full-size spacecraft model was employed in this program; lunar gravity simulation was obtained by applying a force of approximately 5/6 of the spacecraft's Earth weight at the cg in the upward direction through a trailing cable system connected to constant-force pneumatic cylinders.

During the course of this test program, the vehicle was first dropped onto a platform covered with rubber matting. No instability occurred at any of the touchdown velocities of interest. In order to increase the effective coefficient of sliding friction, two-inch cubic abutments were attached to the landing platform. Total instability still did not occur at any landing condition of interest. Three drops were marginally stable. Figure 6 shows the touchdown velocities for these cases.

Although the stability test program did substantiate the conclusion that no danger of landing instability exists unless the specified landing conditions are considerably exceeded, close correlations, in detail, could not be obtained between analytical and experimental stability boundaries (Ref. 3). This is believed to be due primarily to difficulties in the operation of the above mentioned lunar gravity compensation mechanism; furthermore, not all test conditions could be controlled within close tolerances, which applies particularly to the friction between the footpads and the test surface. Undoubtedly, assumptions in the analysis, such as rigidity of the spacecraft frame and a constant coefficient of friction between footpads and ground, have also contributed to the deviation between experimentally and analytically obtained stability boundaries. Hence, the stability boundaries shown in Fig. 6 are not directly comparable. While for the analytical boundary the assumption of a constant friction coefficient of unity was made, the effective friction in the tests was (due to the above mentioned 2 × 2 × 2-in. blocks) not constant and, on the average, considerably higher. However, since generally the landing stability decreases with increasing footpad/ground friction, the experimental results indicate a higher landing capability than was found in the analytical investigation; in other words, the landing stability analysis is, in general, conservative.

Although it was believed that the planar landings include the most critical of all possible landing conditions, an investigation was conducted to explore possible stability degradations due to nonplanar conditions, i.e., non-symmetrical spacecraft attitudes, cross-slope horizontal velocities, and spacecraft tilting in directions other than uphill or downhill. Starting from planar base cases, these effects were introduced in steps throughout their ranges of interest. Investigating all combinations, it was shown that generally any deviation from the base cases resulted in an increased landing stability; however, one exception was found in which a slight degradation is present (Fig. 7). The stability boundary shown in Fig. 7 applies to landings with a horizontal spacecraft velocity (which is variable and serves as the stability indicator)

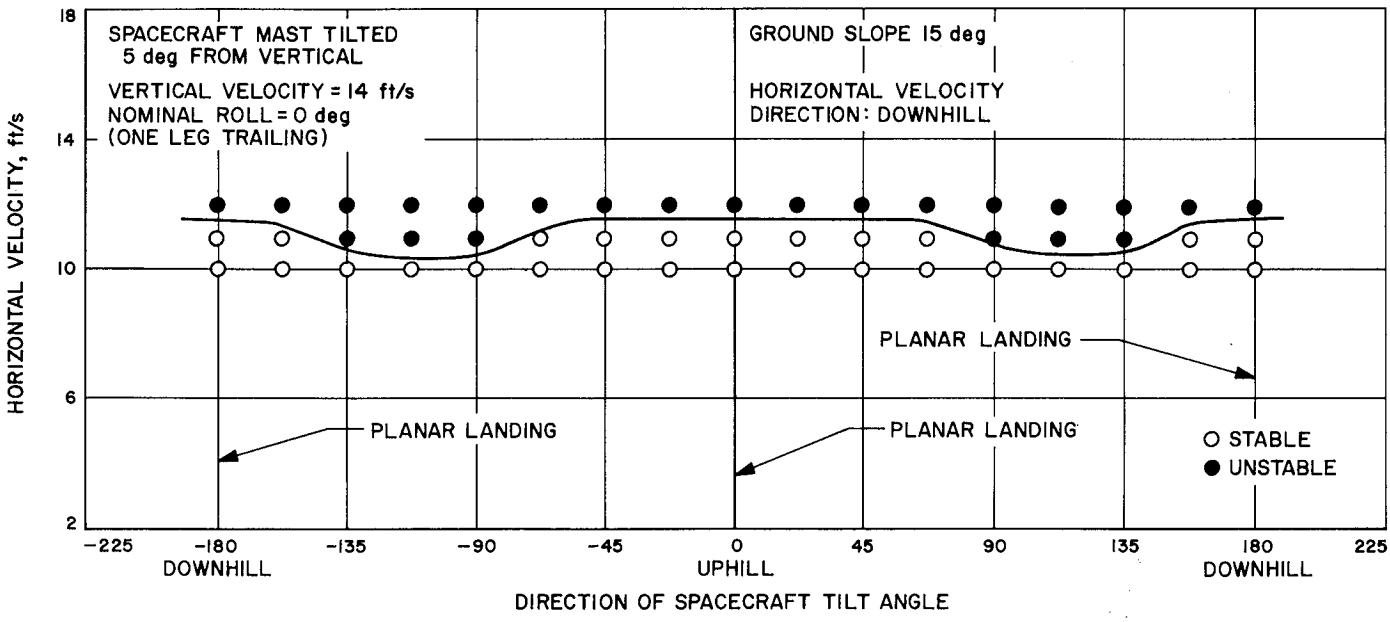

Fig. 7. Degradation of spacecraft stability in nonplanar landings

in the downhill direction, and a symmetrical spacecraft roll attitude (one leg trails). However, a tilt angle of 5 deg between the spacecraft Z-axis and the vertical is introduced, varying in projected direction from 0 deg (uphill) to ±180 deg (downhill) in 22.5-deg steps. As shown, the vehicle will overturn in a landing with 10- to 11-ft/s horizontal velocity if it is tilted between ±90 deg (directly sidewise) and ±135 deg (45 deg off the downhill direction), while it is capable of a stable landing with approximately 1 ft/s more horizontal velocity if the tilt is either uphill or downhill (planar cases). Further investigation showed that this phenomenon disappears as soon as additional nonplanar conditions (cross-slope velocity and nonsymmetric vehicle attitude) are introduced. While this degradation, which is not intuitively obvious, is interesting, it is slight and did not have an impact on the *Surveyor* design because the horizontal velocities are still approximately 50% above the maximum required value.

C. Landing Loads Investigation

Concurrently with the stability investigation, a structure and component landing loads analysis was performed, which was also supplemented by a series of landing tests employing a suitably instrumented full-size structural test vehicle. The analytical approach was based on a modal survey of the structural test vehicle, i.e., an experimental determination of the ten lowest natural frequencies (frequency range from 6 to 70 Hz) and the corresponding mode shapes. Using these as coordinates, the elastic system was represented in 16 uncoupled differential equations (6 rigid body modes plus 10 elastic modes) combined in one matrix equation by use of the so-called generalized mass and stiffness matrices, which then enables a forced response solution for any excitation. Again, landing simulations were performed using as input the force time histories at the six ground contact points obtained in the above described stability program (Ref. 2). This procedure is not entirely consistent because the stability simulation program does not account for elastic responses of the spaceframe and superstructure, i.e., regards the spacecraft main structure as a rigid body with *Surveyor* mass and inertial properties. However, an approximation with deviations generally in the conservative direction is to be expected. Comparisons with test results showed that, in general, a fair agreement was obtained although some deviations were excessive, which is believed to be due to nonlinearities in the structural response, causing some of the off-diagonal terms in the normalized generalized mass matrix to be as high as 0.2. Ideally, all these terms should be zero or very small compared with the unity values in the main diagonal. With accelerations of all important spacecraft components determined by this analysis, it was then possible to estimate stresses in connecting structural members. A more detailed description of the analytical approach is given in Ref. 4.

In regard to the overall vehicle shock loads during landing (i.e., the maximum forces acting on the cg of the spacecraft, assuming a nonelastic main structure), it was shown by this investigation that, even for the most severe of the specified landing conditions, shock loads never reached more than approximately 60% of the specification values of 12 and 30 Earth g in the horizontal and vertical direction, respectively. While this indicates a very satisfactory overall design of the landing system, individual component loads depend, of course, on their location and support structure within the spacecraft, and are generally higher than the cg loads. Peak loads of up to 90 g (Earth) were determined in the antenna/solar panel substructure, and several redesigns, especially in the antenna solar panel positioner, were performed based on results of the load investigation.

Finally, a prototype spacecraft with all components in flight-like configuration and operating, including the telemetry link, was type-approval tested for landing in three drop tests, in order to establish confidence in structural and functional survival of the spacecraft when subjected to the dynamic landing environment.

It was concluded from all these investigations that, from a landing dynamics point of view, the spacecraft was to be expected to survive a landing within the upper three-sigma velocities, provided all systems performed within their design limits and the environmental conditions encountered were within the design specification, i.e., a surface slope of less than 15 deg, no large protuberances or craters, and a fairly firm lunar soil.

IV. Environmental Conditions

A. Lunar Topography

At the time at which the *Surveyor* design specifications had to be generated, including some expected worst-case environmental conditions of the landing site, very little was known about the topography of the Moon on a scale meaningful to *Surveyor*, i.e., to a resolution of the order

of one meter. Judging from large scale data, it was specified that no surface slope in excess of 15 deg was expected and no protuberances higher than 10 cm.

With the successful photographic missions of *Rangers VII, VIII,* and *IX* in 1964 and 1965, a wealth of small-scale topographic data became available through photometric evaluations of the last frames of narrow-angle pictures obtained in these missions (Ref. 5). A statistical analysis was performed simulating a large number of *Surveyor* landings on six *Ranger IX* frames and recording the maximum spacecraft tilt as well as maximum protuberance or depression in the area of the three crushable body blocks (Ref. 6). The results are shown in Figs. 8 and 9, indicating that in more than 97% of all landings a slope of less than 15 deg was encountered, and in 88.5% of all the landings the highest protuberance was 10 cm or less above the plane established by the three foot/surface contact points.

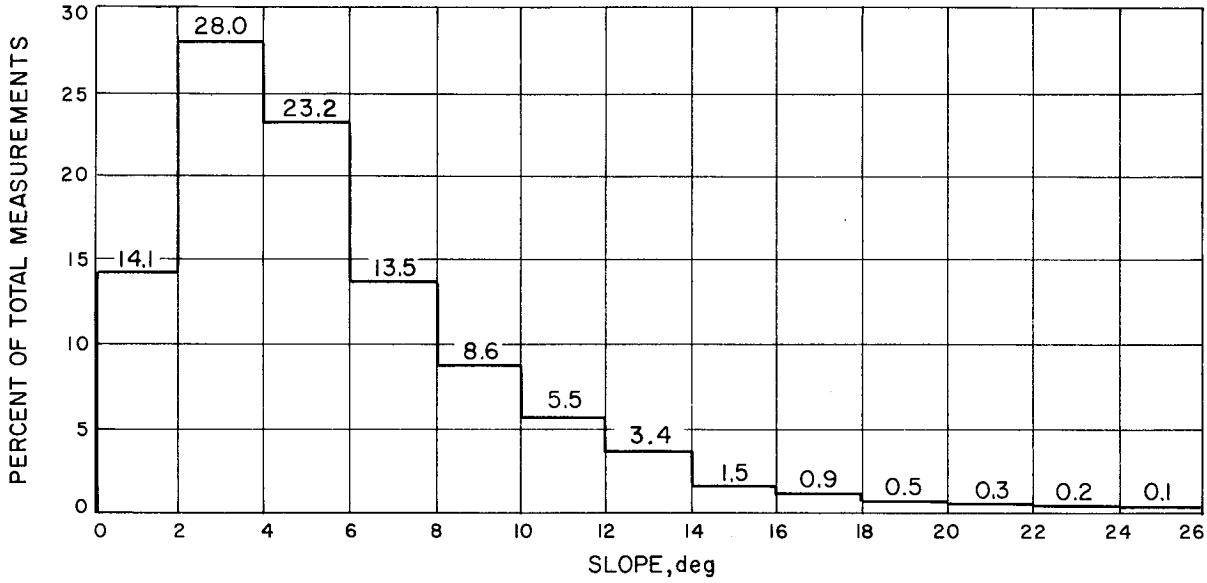

Fig. 8. Average spacecraft tilts for six R9 frames (from Nathan-Rindfleisch data, JPL)

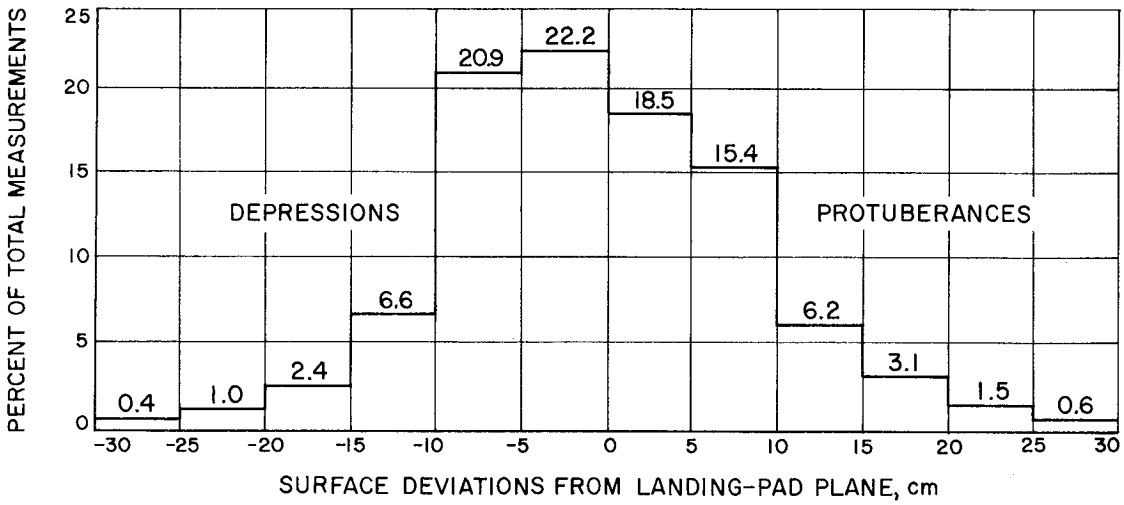

Fig. 9. Frequency distribution of largest depressions and protuberances at points of *Surveyor I* crushable blocks for last R9 P-1, P-3 frames; counting interval, 5 cm

With respect to slopes, the original specification appeared to be an excellent one; with respect to protuberances, it was much less valid. Also, it had become apparent in the meantime that depressions in the area of the body blocks are very undesirable; hence, there was concern about the large number of depressions (10.5% in excess of 10 cm). But in weighing this concern against the implications which would have resulted from a topographical re-specification at that time, it was decided to abstain from such action.

B. Mechanical Surface Properties

If there was little known in regard to small-scale lunar topography at the time of the first *Surveyor* specification, the knowledge about any mechanical properties of the lunar surface was still much smaller. However, at least with respect to the expected hardness of the landing surface, some numerical values had to be provided; this was done by considering two cases, a "hard" and a "soft" surface, specified in the following manner: (1) hard rock, compressive strength 4000 to 25,000 psi, and (2) soft material, compressive strength zero at surface, increasing linearly with depth of vertical penetration at a rate of 10 psi/ft.

Reflected in this all-embracing specification is the fact that, although no direct or indirect measurements were available, there were several scientific models of the lunar surface in existence, suggesting surface hardnesses from hard rock down to 0.05 psi (Ref. 6). This, however, was not much help because, from an engineering standpoint, both extremes had to be considered, the *hardest* for maximum shock environment and the *softest* for landing stability and maximum sinkage. To design for the latter to a value of 0.05 psi (no increase with penetration was given in the scientific model) is next to impossible, which led first to the above considerably harder soft surface specification; later, a lower value of 50 psi for surface bearing strength was adopted for design purposes. However, some analytical and test work was performed assuming the specified soft surface, and while it was established that no sinkage to the point of endangering the functional survival of the spacecraft would result in such material, possible stability degradations were found in cases of downhill landings in which the trailing leg encounters the surface first. Generally, in these cases the two other legs impact with higher impact forces than the first, compressing the material more and therefore effectively increasing the landing slope. Although it was not possible to obtain conclusive test results because of difficulties in finding a soil material with the required characteristics, i.e., the specified compressive strength curve and no spring back, it was strongly indicated that the degradation in landing capability was not substantial enough to offset the comfortable margin which had been established for hard surface landings (see Section III-B).

A hardness of 50 psi which was, as mentioned above, finally adopted as low design value turned out to be equivalent to a rigid surface for the *Surveyor* landing system, because all landings within the specified velocity limits result in a pressure between footpad and ground of less than 50 psi; in fact, a ground force corresponding to 50 psi ground pressure would exceed the force transfer capability of the shock absorber columns. Furthermore, the aluminum honeycomb material of the lower (conical) part of the footpads has a nominal crushing strength of 10 to 12 psi, so that, effectively, a material with more than 10 psi surface bearing strength feels rigid to the *Surveyor* footpads. Hence, design, testing, and analysis of the *Surveyor* system was essentially performed with a rigid landing surface in mind, rigid in this case meaning a surface bearing strength of 10 psi or more.

The first direct indication that there appears to be a reasonable bearing capability at least somewhere on the Moon was provided by the successful landing of Russia's *Luna IX* in February 1966, although no further information facilitating numerical estimates of the bearing strength was obtainable.

C. *Surveyor* Potential for Gaining Knowledge in Regard to Mechanical Surface Properties

Although detailed scientific measurements concerning lunar environmental conditions were to be performed by later suitably equipped *Surveyor* models, it was obviously of great interest to find out as much as possible from the engineering missions, particularly in regard to surface bearing strength. This would be of the highest interest in case the spacecraft should perform successfully the descent and touchdown maneuver but should then fail to survive. In this case, even if only a part of the shock absorber strain-gage data during landing was transmitted, these data would be invaluable for deduction of the encountered ground-reaction forces. A successful landing and survival would render these data less critical but not less interesting, especially because there was a great curiosity within the scientific community as well as the general public to find out, as soon as possible after landing, at least whether the lunar surface was "soft" or "hard."

In order to prepare for this, a method had to be found in which the measured shock absorber forces and the sought footpad/ground forces could be related to each other as reliably and speedily as possible. The relation between these forces is generally quite complex and not necessarily unique; it depends, aside from the soil characteristics, on the spacecraft attitude and velocities at landing. Hence, these variables had to be taken into account, and it appeared that the most reliable way to estimate the ground forces would be to simulate the actual landing analytically, using the spacecraft landing conditions as observed by the RADVS system. By varying the dynamic ground representation, an attempt would then be made to match the analytical shock absorber strain-gage data with the ones observed during the lunar landing. The horizontal and vertical footpad ground forces would then be readily available from the computer simulation.

The main disadvantage of this approach appeared to be the necessity to perform computer runs after data reception before any conclusions could be reached, which would delay the latter by at least several hours if not days. To circumvent this problem, it was decided to conduct a large number of analytical landings prior to touchdown, systematically covering the ranges of expected surface slopes, landing velocities and attitudes, and to assemble the associated shock absorber force history plots in the form of an indexed catalog which would facilitate at least rough data matching immediately after data reception. This was done, resulting in a catalog encompassing 1128 landing cases on a rigid surface, i.e., a surface resisting footpad penetration with at least 10 psi bearing strength. In order to have at least some capability to investigate softer surfaces, a simple soft surface representation in the form of horizontal and vertical ground reaction forces in terms of static and dynamic coefficients was devised, the formulas for which are given and discussed in the following Section V. To repeat all above hard surface cases for different soft surfaces, or combinations of static and dynamic coefficients, proved to be impractical simply because of the excessive number of required computer runs; hence, only selected cases were run for several soft materials in order to be able to judge, generally, the reflection of a low-bearing-strength-material landing upon the shock absorber force data.

For the more detailed data matching program, as mentioned above, all pertinent landing parameters were first to be determined from the spacecraft telemetry in order to limit the program input variables to the soil coefficients. For any landing simulation, nine spacecraft state variables must be known, three linear and three angular velocities, most conveniently in spacecraft coordinates, and three angular positions in an inertial reference system. The first six can be determined from RADVS and gyro data, the latter cannot since the gyro reference is the position of the spacecraft at the 10-ft/s mark, which is not known except for the fact that, by virtue of the gravity turn descent, the spacecraft Z-axis should be close to vertical.

However, these three angles can be determined with respect to a surface based coordinate system. This is achieved by a different application of the landing simulation computer program in which the time differences between the initial impacts of the three footpads, obtained from the shock absorber strain-gage records, are used as an input instead of a pre-specified surface slope and orientation. As a result the relative pitch and yaw angles are obtained as well as the roll angle, if there is any sloping to the reference landing surface; if not, the roll orientation is irrelevant.

Although this gives neither absolute pitch and yaw (with respect to the direction of gravity) nor absolute roll (with respect to lunar north), it is useful for the landing simulation, because, as long as neither the local surface normal nor the spacecraft Z-axis at landing are far off the gravity direction, the relative attitude of the spacecraft with respect to the landing surface is sufficient as an input into the landing program.

The only unknowns still remaining are characteristics of the landing surface. For a rigid surface, there is only one such characteristic, namely the friction coefficient between the footpads and blocks and the lunar soil. In the simulation program, a constant friction coefficient is assumed; hence a straight forward optimization of data match, comparing mission and simulation shock absorber strain-gage records, can be performed by varying this one variable only.

If the ground cannot be regarded as rigid, assumptions will have to be made about the ground reaction forces in their dependence on penetration, penetration velocity, sliding velocity, static and dynamic soil characteristics, and possibly other variables, in order to enable an analytical simulation of the landing process. One such assumption was implemented into the landing-analysis program, as mentioned above and reported in detail in

the following Section V of this report; however, it constitutes only a first rough approach, basically representing the soil by six static and dynamic coefficients. Work is in progress to derive a more refined soil representation, i.e., in terms of such soil characteristics as cohesion, internal friction, relative and absolute density, etc. In any case, however, there will be more than one soil characteristic to be varied in the above described data matching procedure; consequently, there may be more than one "soil" with good data correlation, even though one more piece of information is available for the matching process, namely, the final penetration of the footpads as indicated by TV pictures.

The results of the described short and long term data evaluation for mechanical properties of the lunar surface performed after the first *Surveyor* mission are discussed in Section VII of this report.

V. Computer Simulation

A. Objectives of the Computer Simulation

A digital computer program was developed to study the landing performance of the *Surveyor* spacecraft during the design phase (Ref. 2). The primary objective of this program was to assess the landing stability margins for the *Surveyor* configuration. However, as discussed in Section VII below, a similar landing-simulation program (Ref. 1) was also the primary tool in attempting to estimate lunar surface mechanical properties based on touchdown data obtained from the *Surveyor I* landing.

B. Mathematical Model for Rigid Surface Landings

In the digital computer programs, the *Surveyor* spacecraft is represented by the main body, which is rigid, and the landing gear system. The latter is further broken down into the three articulating inverted tripod legs, three landing feet (footpads), and three crushable blocks (Fig. 2).

Two of the members of the landing leg form the rigid lower strut; the third member contains the hydraulic shock absorber. Mathematically, the shock absorber is described as exhibiting a force which opposes velocity and displacement, and as depending on these two variables in a nonlinear fashion.

The landing foot exhibits a force in the opposite direction of the displacement, this force being a function of the angle of the applied load, the contact area, and the crushing displacement. Due to the footpad geometry, the crushing strength vs displacement is not constant.

The crushable blocks are mathematically similar to the footpads; however, their crushing force is constant.

The landing system geometry and the characteristics of the shock absorbers, the footpads, and the body blocks are described in detail in the Appendix.

In formulating the equations of motion, the following degrees of freedom are considered: 3 translations and 3 rotations of the main body, the 3 angular positions of the individual legs with respect to the main body, and the 3 angular positions of the individual footpads with respect to the legs. The external forces and moments acting on the system are considered to arise from the ground reaction and friction forces, and from gravity.

The above formulation leads to 12 second-order differential equations. The initial solution of these equations establishes a new geometrical configuration of the vehicle which, in turn, determines new forcing functions for the next integration step.

C. Integration Routine

The integration routine used in solving the differential equations of motion is a variable interval, error checking, fourth-order Runge-Kutta integration procedure with a built-in correction for the estimated fifth-order truncation error.

Using this method, the program selects an initial integration interval and performs three integrations, once over the entire interval and twice over two half intervals. By comparing the difference of the two results with a pre-selected allowable truncation error, the time interval is either halved and the process repeated (in case the allowable error was exceeded), or the consecutive integration time interval is increased in proportion to the ratio of allowable error to incurred error (in case the incurred error was below the allowable one).

Not only does this method control the incurred truncation error, but it also allows the integration time interval to be opened up at times when the forcing functions are varying smoothly, thus minimizing computation time.

D. Program Options

In addition to a standard output, the purpose of which is to establish the stability or instability of the vehicle, several other optional outputs are available. These options provide complete time histories of spacecraft motion, landing loads acting on the landing gear and the main structure, and a detailed breakdown of dissipated energies.

A further option was implemented to aid in the interpretation of lunar data. This option accepts in addition to the standard input (spacecraft geometry, inertial properties, and initial conditions of the impact) the touchdown times of the three footpads. The program will then, utilizing these times, calculate the effective slope on which the spacecraft landed and the vehicle orientation with respect to this slope at the time of touchdown. This information can then be used, in connection with telemetry data, to attempt a complete analytical simulation of the actual lunar landing.

E. Modification for Non-Rigid Surface Landings

In order to provide some capability in handling non-rigid surface landings, a modified version of the landing program was devised. In this modified program, the footpads have been removed, the body blocks are noncrushable, and the ground reaction forces (F_v) and friction forces (F_h) acting on the footpad pivot points and on the body block face plates are functions of certain soil constants ($C_1 \ldots C_6$), vertical penetration into the soil (x), vertical penetration velocity ($\dot{x}$), horizontal displacement (y), and sliding velocity ($\dot{y}$) as expressed in the following two equations:

$$F_v = C_1 + C_2 x + C_3 \dot{x}^2$$

$$F_h = C_4 x \dot{y}^2 + C_5 F_v + C_6 x$$

In the vertical force equation, C_1 represents the static surface resistance of the top surface layer, while C_2 indicates the linear increase of this resistance with vertical penetration, and C_3 is to account for any increases in the vertical ground force due to dynamic effects during footpad impacting. In the horizontal force equation, the term associated with C_5 can be recognized as representing a conventional surface friction force, while the C_6 and C_4 terms are designed to account for static and dynamic effects, respectively, resulting from horizontal motions of the footpad while penetrating vertically into the surface material.

VI. *Surveyor I* Performance

The performance of *Surveyor I* during the final descent and landing phase was, in general, very close to nominal. The three landing strain-gage bridges, mounted on the shock absorber columns of the three landing legs, returned excellent analog force vs time traces. A reproduction of these traces is shown in Fig. 10. They indicate that the three landing legs contacted the lunar surface with the following time intervals and maximum forces:

Leg 2: 0.000 s (ref) ; 1600 ±80 lb

Leg 1: +0.005 ±0.001 s ; 1390 ±70 lb

Leg 3: +0.018 ±0.001 s ; (1400 ±70 lb)

There is some uncertainty in the calibration of the Leg 3 channel; hence, the peak force, calculated under the assumption that all systems associated with this measurement performed nominally, is given in parentheses.

The maximum forces occurred approximately 120 ms after impact, followed by a rapid force decrease. At approximately 0.5 s after impact, all three channels show zero force, indicating that the spacecraft rebounded off

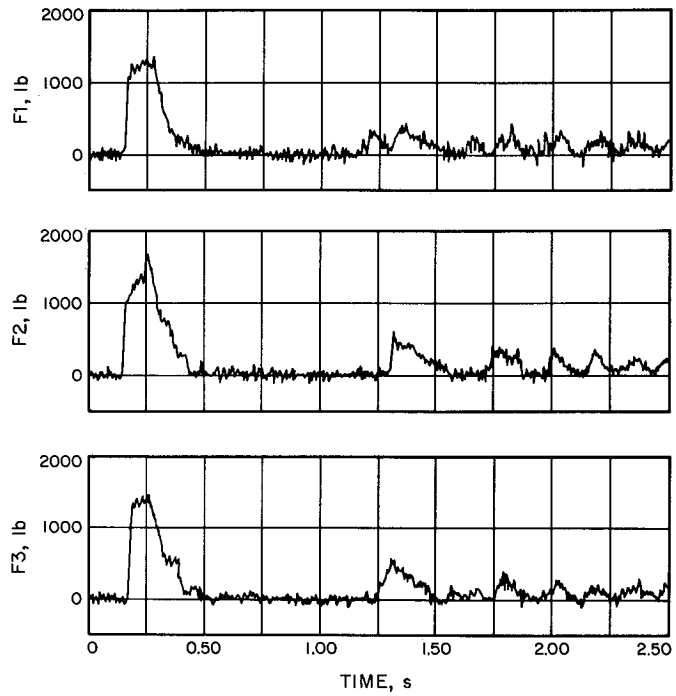

Fig. 10. *Surveyor I* shock absorber strain-gage force histories

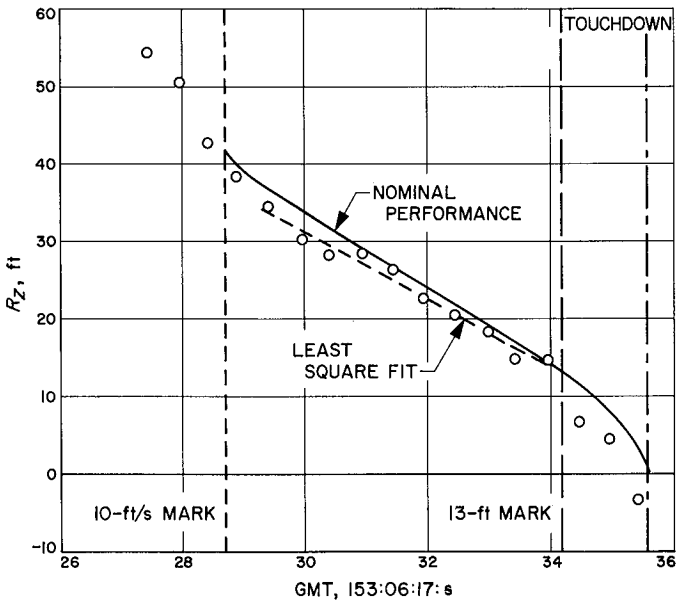

Fig. 11. *Surveyor I* RADVS range data

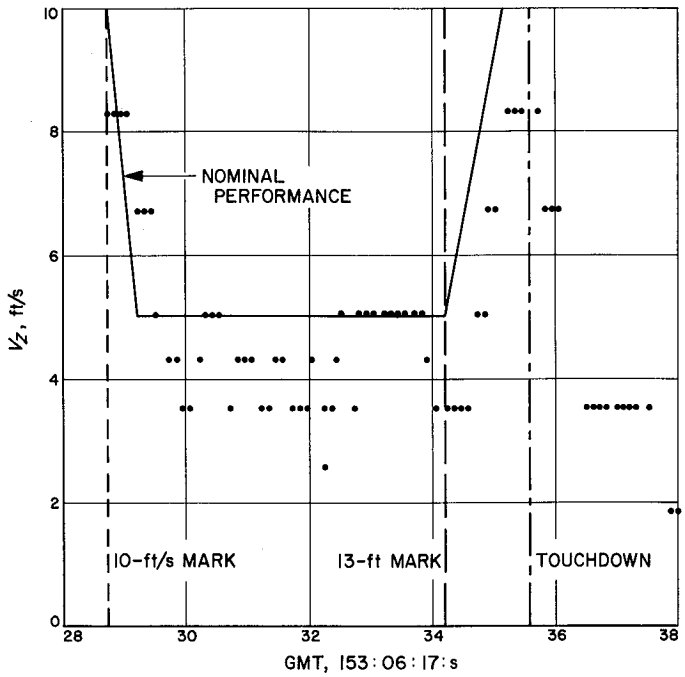

Fig. 12. *Surveyor I* RADVS velocity data, V_z

the lunar surface. A second impact is registered approximately 1.1 to 1.2 s after the first. Maximum forces developed in the second impact reached approximately the 400-lb level. It was predicted that the body blocks would also contact the surface under the encountered landing conditions. Several TV pictures show block imprints in the lunar surface, confirming that block contact did occur.

The digital telemetry returned by *Surveyor I* was also very good, enabling close estimates of *Surveyor I* performance parameters. Figure 11 shows the RADVS range data, the dots indicating flight measurements; the dashed least-squares-fit straight line was established based on measurements 2 through 11 between the 10-ft/s mark and the 13-ft mark (vernier engine cutoff); the first point after the 10-ft/s mark was not used because the preprogrammed constant descent velocity of 5 ft/s cannot be reached before approximately 0.3 to 0.4 s after command (10-ft/s mark). Actually, as indicated by the slope of the dashed line, the constant descent velocity was approximately 4.3 ft/s. This value is indicated directly by the RADVS V_z data shown in Fig. 12. However, the accuracy of the RADVS telemetry in regard to velocities during the terminal descent phase is not very high. Fortunately, the timing of discrete events is indicated quite accurately in the telemetry, affording much more reliable estimates for the touchdown velocities, provided the spacecraft angular position at vernier engine cutoff can be determined. One input for this is given by the gyro data (Figs. 13 and 14). Here, it can be seen that very little angular motion in pitch and yaw took place between the 10-ft/s mark and touchdown. However, only relative information is provided by these data, because the gyros are referenced to the spacecraft attitude at the start of the inertial hold mode (10-ft/s mark); and this attitude is not known except that, due to the preceding gravity-turn descent, the spacecraft Z-axis should be close to vertical. But a true reference can be obtained by star sightings, which were performed during *Surveyor I* lunar surface operations, from which a flight path angle of 1.8 deg off vertical at vernier engine cutoff was estimated. With this information and the timing of events obtained from spacecraft telemetry (vernier cutoff from digital data, touchdown from strain-gage data, both recorded together with a NASA 36-bit standard time code affording mutual time reference), the vertical and horizontal landing velocities can be calculated using free-fall relations; in addition, the indicated time difference between the 10-ft/s and the 13-ft mark has to be taken into account because a slight horizontal velocity component is introduced due to vernier thrusting during this period with the spacecraft inertially fixed in attitude, i.e., remaining at the flight path angle which it had reached at the time of the 10-ft/s mark.

A summary of actual and predicted landing performance parameters is shown in Table 1. The predicted maximum shock absorber force is based on a hard surface landing and constitutes an upper bound, since the

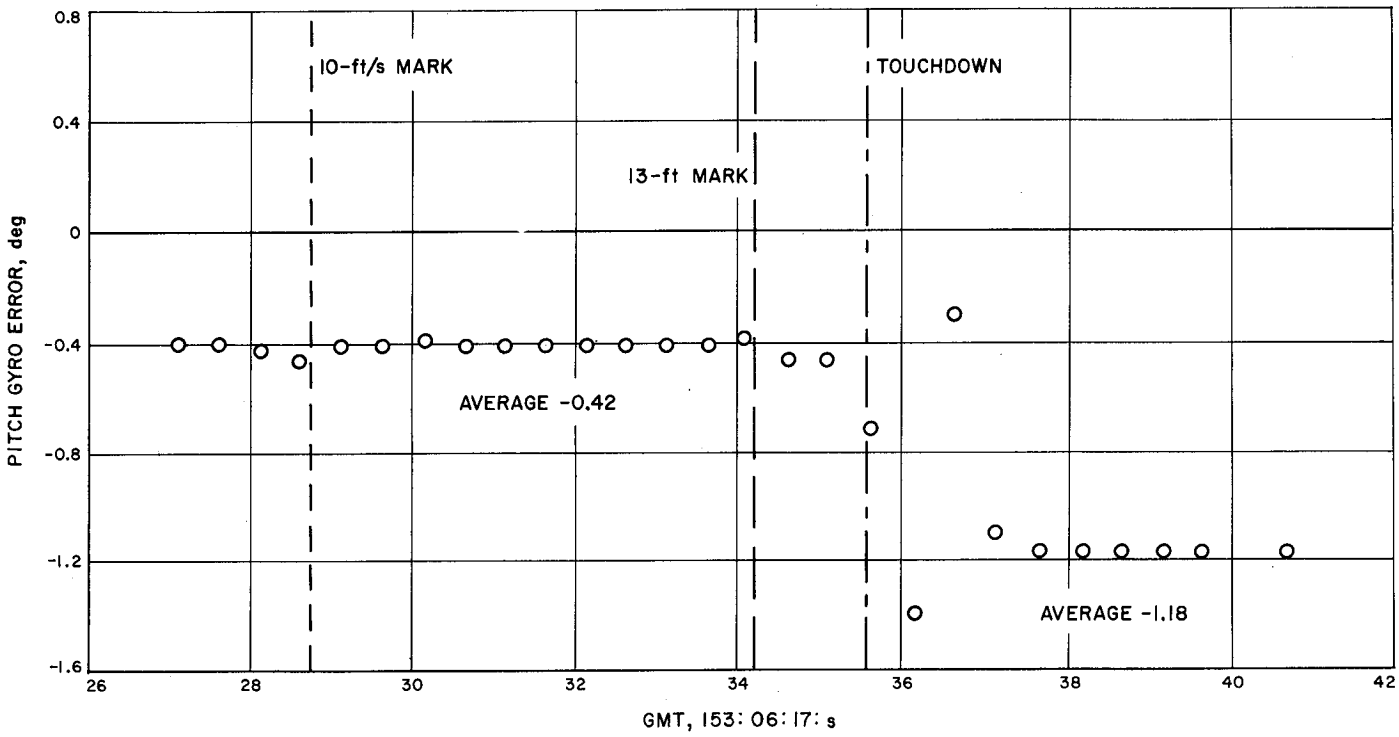

Fig. 13. *Surveyor I* pitch gyro data

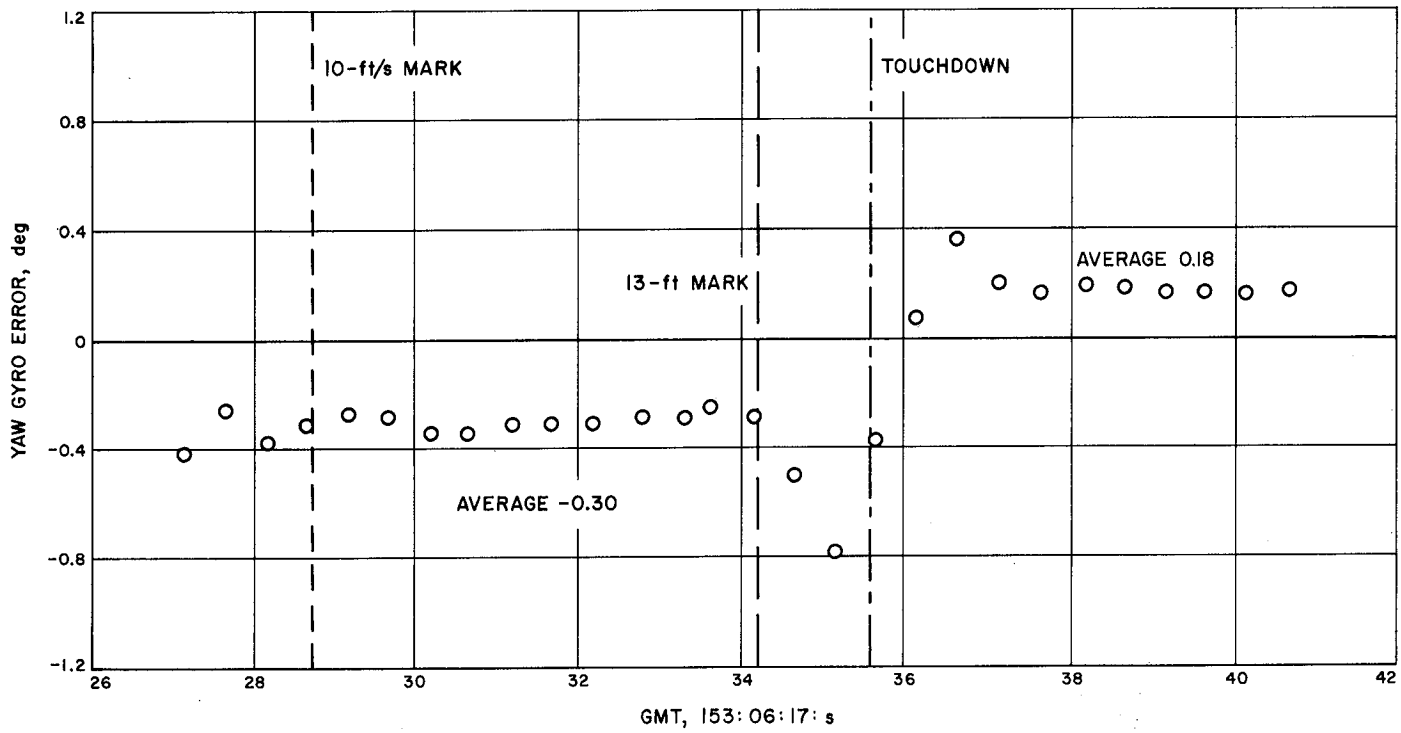

Fig. 14. *Surveyor I* yaw gyro data

Table 1. Summary of actual and predicted landing performance parameters

Parameter	Units	Predicted	Actual
Horizontal landing velocity	ft/s	< 5.0	0.8 ± 0.3
Vertical landing velocity	ft/s	12.6 ± 2.5	11.6 ± 0.4
Vertical velocity at engine cut-off	ft/s	5.0 ± 1.5	4.3 ± 0.2
Altitude at engine cut-off	ft/s	13 ± 4.5	10.8 ± 0.3
Peak shock absorber force	lb	< 1770	1600 ± 80
Flight path angle at landing	deg	< 7.0	1.8 ± 0.5
Angular velocity at landing	deg/s	< 3.2	< 1.0

landing simulation program does not take account of the flexibility of the spaceframe and superstructure which, by absorbing some of the energy dissipated at landing, tends to decrease the shock absorber forces. Figure 15 shows the actual conditions at vernier engine cutoff within the three-sigma prediction ellipse.

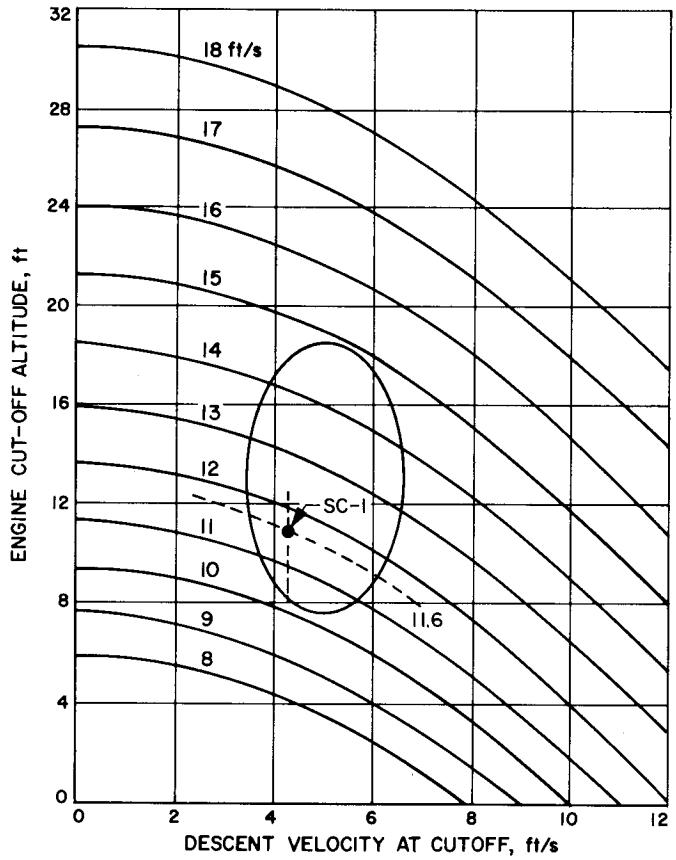

Fig. 15. Three-sigma ellipse showing predictions in descent velocities and engine cutoff height

The landed Earth weight of *Surveyor I* was 643.3 lb. Except for a slightly stronger than expected spacecraft rebound, the landing occurred well within predicted performance parameters, no structural or functional damage was encountered due to the landing shock; in one respect, this shock was even advantageous to the mission: omni-antenna A, which was indicated not to have deployed during transit (the pyrotechnic pin puller had functioned properly, but there was apparently excessive friction in the holddown fixture), was shaken loose by either the retro motor deceleration or the landing impact, and latched into its proper position.

VII. *Surveyor I* Landing Data Evaluation and Interpretation

A. Short-Term Data Evaluation

Except for TV pictures, the first data of directly intelligible form which became available after *Surveyor I* touchdown were the three shock absorber force histories. The first oscillographs of these data, obtained at the JPL Space Flight Operations Facility (SFOF) in Pasadena which is connected with the Goldstone Tracking Station by microwave link, contained considerably more noise than the ones which were later obtained directly from the Goldstone magnetic tape. However, the quality of the first graphs was sufficient to allow the following preliminary conclusions:

(1) The spacecraft landed in an attitude in which its mast was within 1 to 2 degrees normal to the landing surface. This conclusion was based on the short time intervals between leg impacts, approximately 5 and 15 ms, respectively. The catalog showed time differences of 70 to 100 ms for a 7.5-deg angle between spacecraft mast and local surface normal, 100 to 190 ms for a 15-deg angle.

(2) The surface material in which *Surveyor I* landed appears to be dynamically "hard," i.e., a surface bearing strength in the order of 10 psi was encountered by the footpads within milliseconds after impact. This conclusion was based upon an examination of initial rise characteristics in the force histories which were very similar to the ones shown in the hard surface landing simulations with approximately the same force peak values. (See Fig. 16.)

(3) The vertical landing velocity was between 9.0 and 12.5 ft/s, closer to the upper limit, and the horizontal landing velocity was approximately 0 ft/s.

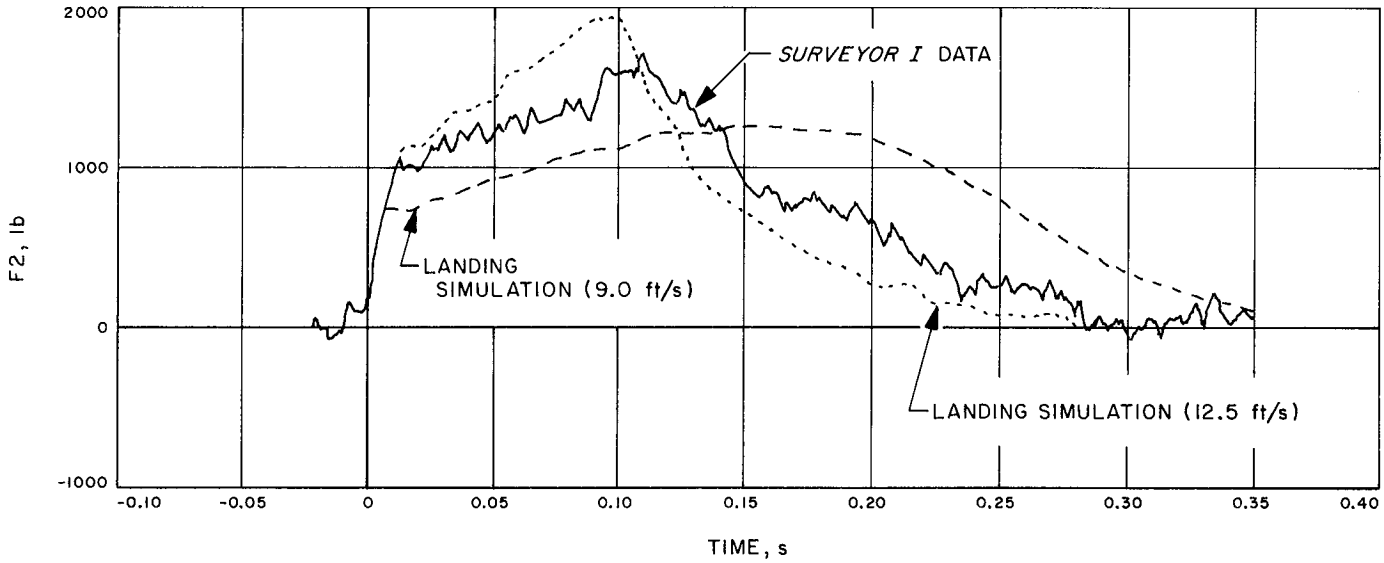

Fig. 16. Bracketing of *Surveyor I* strain-gage data by pre-mission catalog landing cases (Leg 2)

This conclusion was reached by finding closest resemblance with the corresponding cases in the landing catalog. (See Fig. 16.)

In connection with footpad TV pictures, which show some penetration into the surface material, it could also be concluded that the surface, although it reacted dynamically like a "hard" surface, is not rock-like but rather like fairly loose granular soil, at least in its upper few centimeters, with a bearing capacity of less than 10 psi in its very top layer. Preliminary results of this investigation are published in Ref. 7.

B. Long-Term Data Evaluation

The first step in the long term data evaluation was to establish the landing velocities and attitude based upon RADVS telemetry, event timing, landing simulation based on leg impact timing (this option of the landing simulation program is described in Section V-D) and, finally, star sightings. The results are shown in Table 1; the angle between the (planar) landing surface and a plane containing the three footpad pivot points at initial touchdown was established to be 1.2 deg.

With the thus established initial conditions, several rigid surface landing simulations were performed assuming a range of surface friction coefficients. While there were no manifest differences, it appears that a friction coefficient of unity yields shock absorber force histories closest resembling the flight data. The comparison for Leg 2 is shown in Fig. 17, which can be seen to be quite close. However, a more detailed comparison with respect to maximum force, elapsed time between zero and peak force, pulse width at half-peak force, and elapsed time between first and second impact showed some distinct deviation; also, it was evident from TV pictures that the surface is not absolutely rigid, hence a better data match was being sought by use of the soft-surface landing simulation capability described in Section V-E, above.

It is realized that this soil force representation is very crude and might, due to inability to simulate actual soil behavior, result in worse rather than better flight data correlations, or, even if it does correlate well, not necessarily lead to valid conclusions. Very little work has been done in the field of slow impact soil dynamics, and while the suggested force equations are in a form enveloping whatever results from pertinent investigations are available, this does not prove their ability to represent actual soil reactions, especially in connection with a material of largely unknown properties.

However, for the following discussion it will be assumed that the employed soil reaction equations constitute approximations which may be rough but are basically valid; until presently performed soil studies provide better reaction force equations, this is the only course that can be taken in order to reach any conclusions at all.

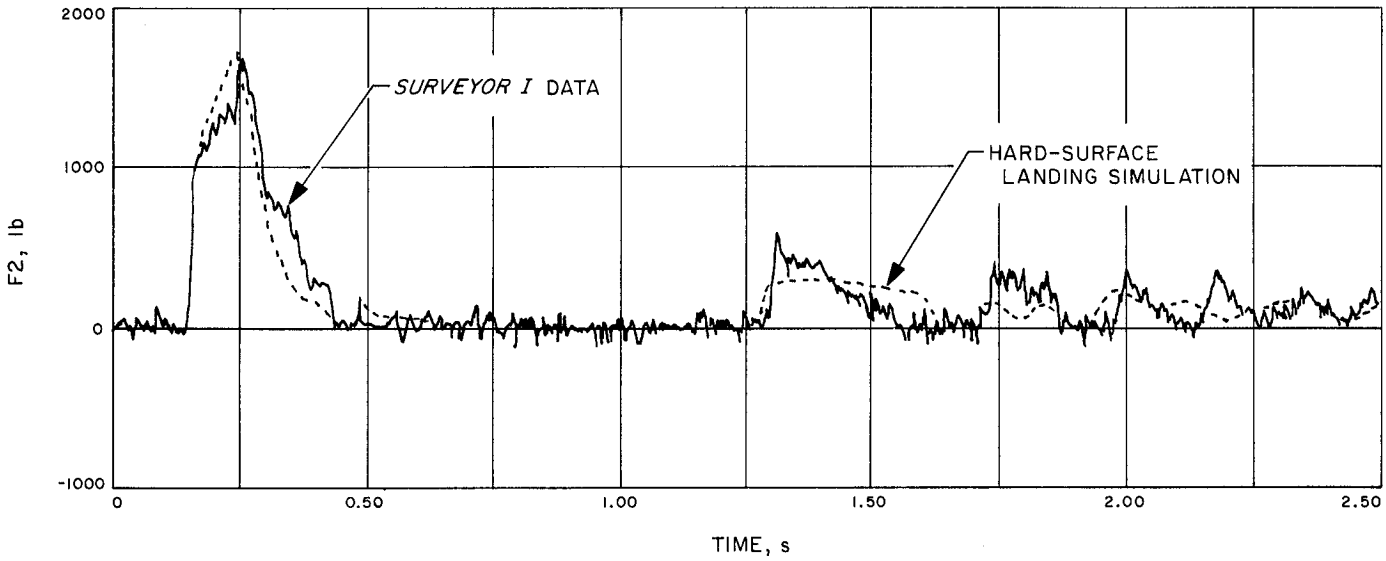

Fig. 17. Comparison of *Surveyor I* strain-gage data with post-mission hard surface landing simulation (Leg 2)

Due to the very low horizontal landing velocity of *Surveyor I*, it was decided to neglect any effects from footpad "plowing," i.e., to assume the coefficients C_4 and C_6 in the horizontal force equation (see Section V-E) to be zero.

After setting reasonable upper and lower bounds for the remaining coefficients C_1, C_2, C_3, and C_5, as described below, a parametric computer study was performed, varying these four coefficients.

Due to the truncated cone shape of the footpads, C_1 and C_2 do not directly correspond to a constant and a linearly penetration-dependent surface-bearing strength, respectively. Instead, a certain C_1/C_2 combination is used to approximately represent a soil of constant bearing strength; a soil with a linearly increasing bearing strength (x is the vertical penetration)

$$\sigma = \alpha + \beta x$$

can then be approximated by increasing C_2 above the value required for the constant bearing-strength soil. Numerically, the relation between the vertical ground reaction force

$$F_v = C_1 + C_2 x$$

and the above bearing-strength equation is

$$C_1 \approx 50\alpha;\ C_2 \approx 31.25\alpha + 75\beta$$

with the following dimension convention

$$\sigma, \alpha\ (\text{psi});\quad \beta\ (\text{psi/in.});\quad x\ (\text{in.});\quad F_v, C_1\ (\text{lb});\quad C_2\ (\text{lb/in.})$$

Due to the footpad configuration (see Appendix, Fig. A-1), these relations apply up to two inches of vertical penetration, which, however, covers the range of interest since the best estimates of *Surveyor I* footpad penetrations are:

Pad 2 penetrated approximately 2.0 in.

Pad 3 penetrated approximately 1.8 in.

(Pad 1 is outside the camera field-of-view.)

To return to the setting of bounds, obviously

$$0 \leq \alpha \leq 10\ \text{psi}$$

can be assumed since a top surface-layer bearing strength of greater than 10 psi would have resulted in footpad crushing rather than penetration, except for the lunar surface crust model, i.e., a thin hard crust overlaying a much weaker material. Since it appears that there was no footpad crushing at all, even after penetrating (although this cannot be definitely established), an upper bound of

$$\alpha + \beta x \leq 10\ \text{psi}$$

seems reasonable, especially since some increase in force is to be expected from the dynamic term $C_3\dot{x}^2$. This, again, excludes the crust model or any other material with a negative β, i.e., a decrease in bearing strength with progressing penetration. While such model cannot be ruled out definitely, there is nothing in the *Surveyor I* data which would support it, and it was not considered in this investigation.

To bracket the dynamic factor C_3, a rough estimate based on the apparent volume of displaced material, the throw-out pattern, and estimated timing (using a conservative density value of 3 g/cm^3) resulted in an upper value of approximately 2.5 lb-s^2/ft^2. Finally, the friction coefficient C_5 was estimated to lie between approximately 0.5 and 1.5.

Several trends became apparent in the initial stage of the computer study which consisted of approximately 80 runs. First, while the output in form of shock-absorber force time plots was somewhat sensitive to changes in α and β values, footpad penetration values appear to be a more critical indicator. Neither one, however, is very sensitive to changes in friction as well as the above-mentioned dynamic factor C_3 within their established bounds. While the latter resulted in high initial normal forces on the footpads, as is to be expected, these forces are of very short duration and seem not to influence the shock absorber force histories or the penetration values in a significant way.

As a result, it was decided to neglect this ground inertia effect, i.e., assume $C_3 = 0$, and to continue the investigation with a friction coefficient of 0.7, which appeared to be most reasonable, although, as mentioned, changes in this value also resulted in almost unnoticeable changes in the program output.

Hence, it appears that the only variables of importance are α, the top layer static bearing strength, and β, the linear increase in static bearing strength with vertical penetration.

A second computer study was then performed, consisting of about 60 runs, varying α and β only. The selection of strain-gage recordings and footpad penetrations resembling the flight data best was finally narrowed down to the numerical values $\alpha + \beta = 4$ and $\alpha + \beta = 3$, all integer combinations of which are displayed in Fig. 18 together with the *Surveyor I* record. Leg 2 was again used for comparison because it impacted first and is, therefore, believed to indicate soil conditions best. As can be seen, all simulations show reasonable agreements in peak forces, time behavior, and maximum footpad penetrations, and it is questionable whether any further selection process is justified in view of the crudeness of the soil model and the subtle deviations evident in Fig. 18. Apparently, the data are not sufficient and/or the method not adequate to distinguish definitely between a material with a fairly constant bearing capacity and one which has a marked increase in bearing strength with vertical penetration. However, a close comparison of the initial impact pulse shapes appears to favor the models with an increasing bearing strength, as it is quite evident when comparing the $\alpha = 0$, $\beta = 4$ simulation (increasing bearing strength) with $\alpha = 4$, $\beta = 0$ (constant bearing strength), or $\alpha = 0$, $\beta = 3$ with $\alpha = 3$, $\beta = 0$; in fact, it seems that an even higher increase would approximate the pulse shape better; however, in the employed linear soil model, this would result in too little footpad penetration. This then suggests that a soil model featuring a bearing-strength increase proportional to x^a (x = vertical penetration) with $a > 1$ can be expected to correlate better with the *Surveyor I* flight data. Although it would not have been difficult to modify the landing computer program accordingly, this was not done because a much more refined soil representation is expected to be available soon; this soil model will be based on physical soil properties such as cohesion, density, internal friction, particle size distribution, etc., and is therefore expected to be superior to the above used static and dynamic coefficient approach. (The work referred to is being performed for NASA by the Bendix Products Aerospace Division, South Bend, Ind.)

In concluding the soil discussion, it may be said, with all the necessary precautions pointed out above, that, based on the outlined investigation, the following bearing-strength characteristics appear most likely to be prevailing on the lunar surface at the *Surveyor I* landing site: the bearing capability of the lunar surface material is between 0 and 2 psi in the uppermost layer. When penetrated (i.e., compressed and/or displaced) by a flat circular object with an 8- to 12-in. diameter, the bearing capability increases more rapidly than the penetration, reaching a value between 6 and 8 psi at a depth of approximately 2 in. Whether this increase is due to material compaction or to the presence of layers with different original strength characteristics cannot be decided from the above presented investigation.

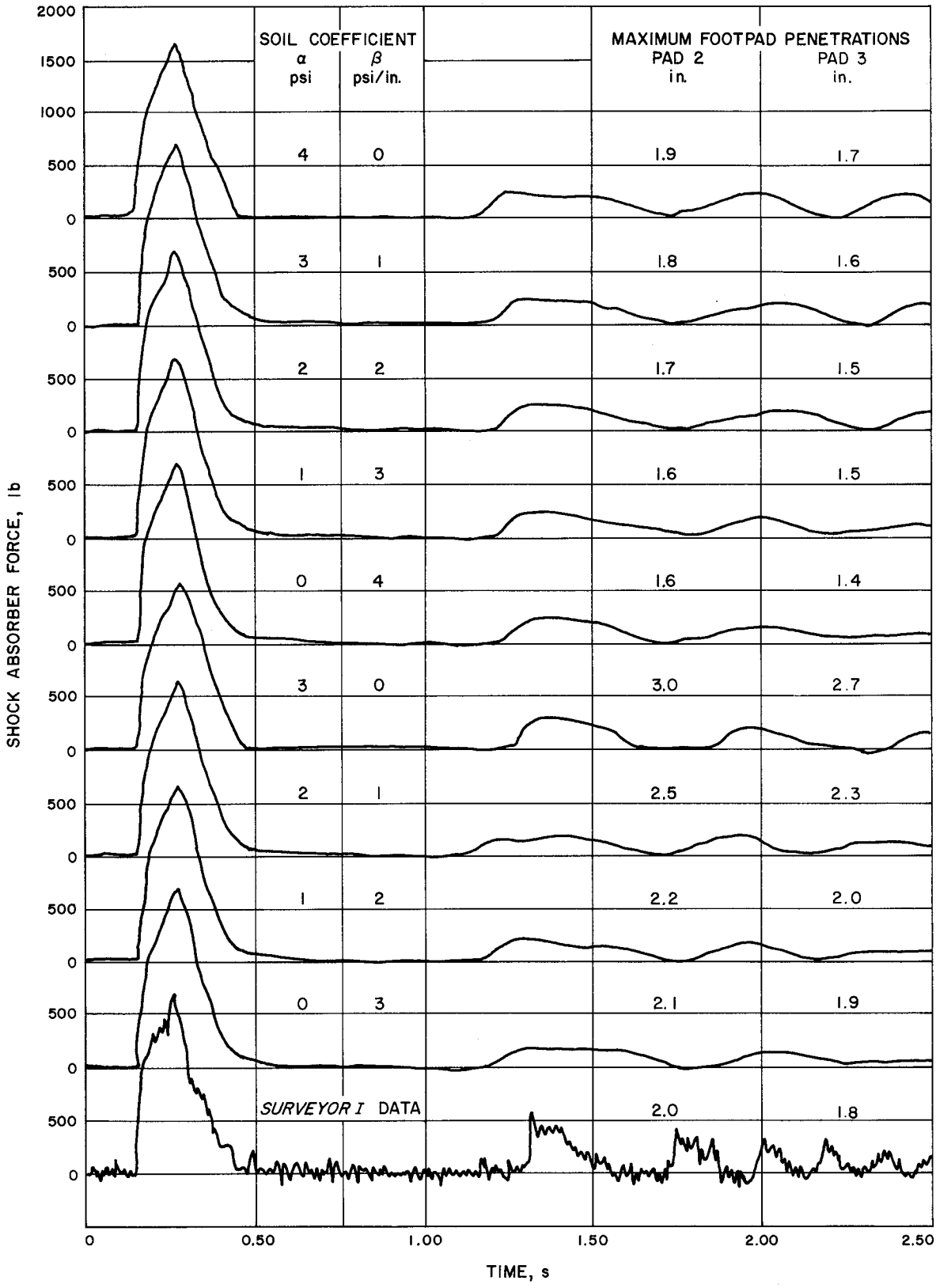

Fig. 18. Soft surface landing simulation (Leg 2)

Appendix
Landing-Gear Characteristics

This Appendix describes the landing-gear characteristics as they are modeled in the computer simulation. The landing-gear system geometry and the shock-absorber characteristics apply to both the rigid surface and the nonrigid surface versions of the landing program. In the nonrigid surface version of the program, the footpads and body blocks are not allowed to crush. Hence, the footpad and body block characteristics described in this Appendix apply only to the rigid surface version of the program.

I. Landing-Gear Geometry

The pertinent geometry of the landing gear system is shown in Fig. A-1.

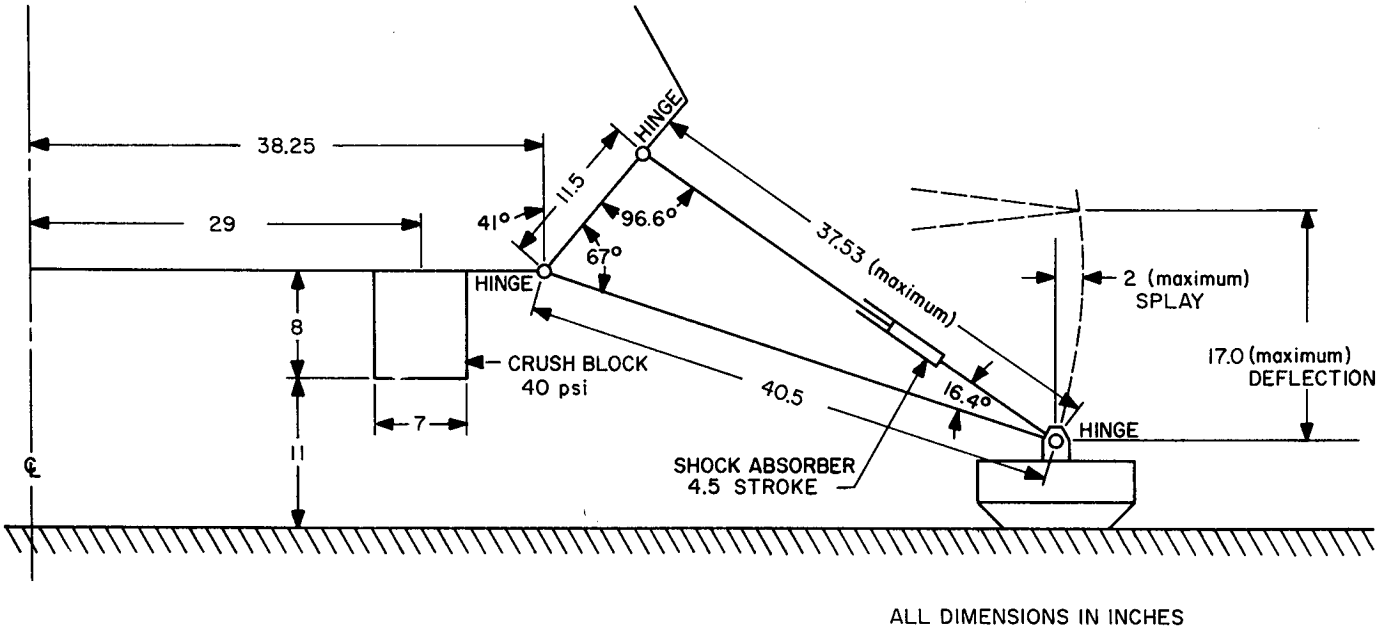

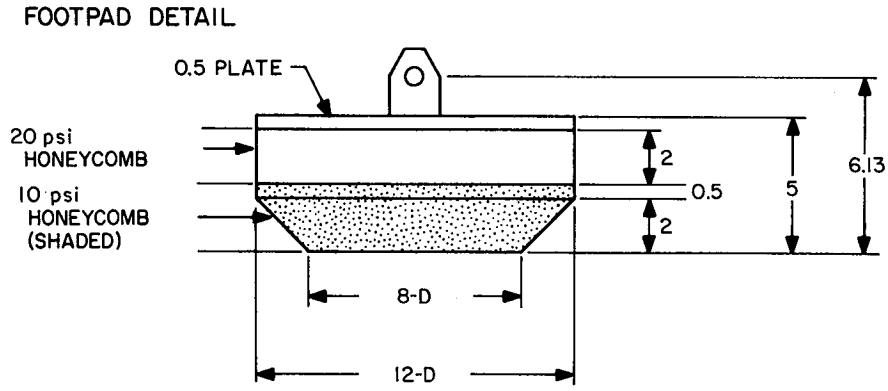

Fig. A-1. *Surveyor I* landing gear geometry (shown fully extended), and footpad detail

II. Shock-Absorber Characteristics

After the initial compressive strain due to the preload is overcome, the shock-absorber force is given by

$$F_s = K_D S_k\left(\delta - \frac{F_P}{K_s}\right) + F_P - \nu \frac{\dot{\ell}_D}{|\dot{\ell}_D|}\left|K_D S_k\left(\delta - \frac{F_P}{K_s}\right) + F_P\right| - \dot{\ell}_D |\dot{\ell}_D| R_D S_D$$

where

F_s total shock-absorber force, lb

K_D spring constant of hydraulic spring, lb/ft

S_k profile to give nonlinearity of spring constant as a function of shock-absorber stroke, dimensionless

δ deflection of shock absorber, ft

F_P hydraulic spring compressive preload, lb

K_s axial stiffness of strokable strut, lb/ft

ν mechanical friction coefficient of shock-absorber moving parts, dimensionless

$\dot{\ell}_D$ rate of change of shock absorber length, ft/s

R_D damping constant, lb-s²/ft²
$R_D = R_C$ for compression
$R_D = R_R$ for rebound

S_D profile to give nonlinearity of damping constant, dimensionless
$S_D = S_C$ for compression
$S_D = S_R$ for rebound

Typical shock absorber profiles are shown in Fig. A-2. This figure shows the nominal characteristics as specified to the manufacturer. Each flight shock absorber assembly was tested at room temperature.

The following numerical values obtained from these tests were used in the computer simulation to describe the shock-absorber characteristics. Where applicable, K_D, F_P, R_C, and R_R have been adjusted according to estimates of the individual landing-leg temperatures at touchdown.

Leg 1:

$K_D = 3330$ lb/ft $\quad R_C = 60$ lb-s²/ft²
$F_P = 240$ lb $\quad R_R = 800$ lb-s²/ft²
$K_s = 100{,}000$ lb/ft $\quad \nu = 0.05$
$S_L = 2.505$ ft⁻¹

Leg 2:

$K_D = 3760$ lb/ft $\quad R_C = 61.8$ lb-s²/ft²
$F_P = 220$ lb $\quad R_R = 1000$ lb-s²/ft²
$K_s = 100{,}000$ lb/ft $\quad \nu = 0.05$
$S_L = 2.025$ ft⁻¹

Leg 3:

$K_D = 3820$ lb/ft $\quad R_C = 47.5$ lb-s²/ft²
$F_P = 217$ lb $\quad R_R = 965$ lb-s²/ft²
$K_s = 100{,}000$ lb/ft $\quad \nu = 0.05$
$S_L = 2.280$ ft⁻¹

The axial stiffness of the shock-absorber column, K_s, was reduced from 100,000 to 25,000 lb/ft for the computer simulations employing the soft-surface model (Fig. 18). This was done to represent the structural stiffness of the entire undeflected leg set which is critical for the initial rise characteristics of the shock-absorber-force time histories. The revised value is based on a static deflection test conducted with a flight-like leg assembly.

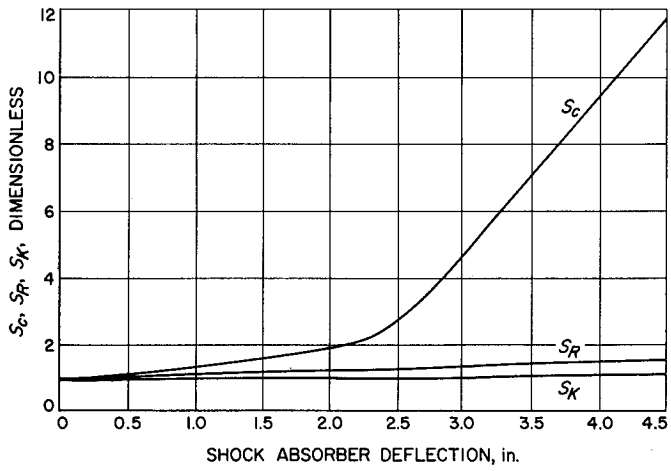

Fig. A-2. Typical shock absorber spring and damping profiles

In the computer program, the profile S_R is specified as a straight line having a value of 1.0 at zero deflection and a slope of S_L. The profiles S_C and S_k are supplied to the computer in tabular form as shown in Table A-1.

Table A-1. Shock absorber characteristics

Shock-Absorber Deflection, in.	Leg 1		Leg 2		Leg 3	
	S_k	S_C	S_k	S_C	S_k	S_C
0	1.0	1.0	1.0	1.0	1.0	1.0
0.25	1.0	1.025	1.0	1.050	1.0	1.12
0.50	1.0	1.050	1.0	1.075	1.0	1.45
0.75	1.0	1.075	1.0	1.170	1.0	1.55
1.00	1.0	1.100	1.0	1.170	1.0	1.67
1.25	1.0	1.200	1.0	1.330	1.0	1.75
1.50	1.0	1.330	1.0	1.450	1.0	1.99
1.75	1.009	1.430	1.013	1.570	1.0	2.20
2.00	1.016	1.550	1.027	1.730	1.0	2.30
2.25	1.019	1.750	1.022	1.970	1.0	2.63
2.50	1.031	2.100	1.025	2.470	1.0	3.33
2.75	1.039	2.880	1.034	3.550	1.021	4.65
3.00	1.046	3.750	1.039	4.630	1.035	6.14
3.25	1.057	4.880	1.042	5.670	1.039	7.24
3.50	1.059	5.500	1.052	6.750	1.058	8.68
3.75	1.067	6.300	1.066	8.100	1.051	10.03
4.00	1.074	7.170	1.081	9.050	1.066	11.42
4.25	1.082	8.220	1.090	10.380	1.071	12.87
4.50	1.089	9.180	1.102	11.520	1.081	14.29
6.50	1.148	16.860	1.185	20.640	1.161	25.65

Linear interpolation is used between the listed values.

III. Footpad Characteristics

The crush force acting on any segment of the footpad is given by

$$F_f = A_c\, C_f\, P_c \left(\frac{0.75 + 0.25 \cos 2\xi_f}{\cos \xi_f} \right)$$

where

F_f crush force acting normal to the ground surface, lb

A_c contact area, ft²

C_f nominal crushing strength per unit area, lb/ft²

P_c profile to give variation in crushing strength per unit area with displacement, dimensionless

ξ_f angle of applied load from crushable structure axis, deg

The following numerical values, corrected for estimated individual footpad temperatures at touchdown, were used in the computer simulation:

Footpad 1: $C_f = 1640$ lb/ft²

Footpad 2: $C_f = 1640$ lb/ft²

Footpad 3: $C_f = 1687$ lb/ft²

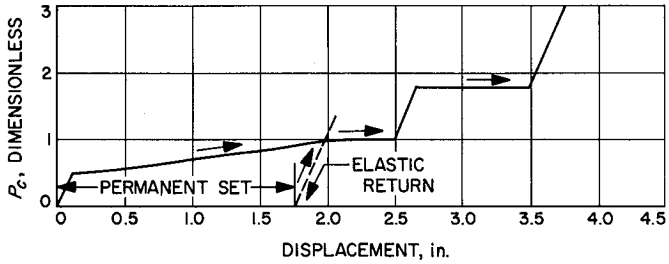

Fig. A-3. Typical footpad crush pressure profile

The profile P_c is shown in Fig. A-3. It is supplied to the computer in tabular form as shown in Table A-2.

Table A-2. Footpad characteristics

Displacement, in.	P_c
0	0
0.10	0.468
0.25	0.502
0.50	0.563
0.75	0.629
1.00	0.697
1.25	0.767
1.50	0.841
1.75	0.920
2.00	1.00
2.49	1.00
2.66	1.823
3.50	1.823
4.50	6.503

Linear interpolation is used between the listed values.

The profile P_c given above applies to each of the three footpads.

IV. Body-Block Characteristics

The crush force acting on the crushable body block is given by

$$F_B = A_B C_B P_B (0.75 + 0.25 \cos 2\xi_B)$$

where

- F_B crush force acting normal to the ground surface, lb
- A_B contact area, ft²
- C_B nominal crushing strength per unit area, lb/ft²
- P_B profile to give variation in crushing strength per unit area with displacement, dimensionless
- ξ_B angle of applied load from crushable structure axis, deg

The following numerical values, corrected for estimated individual body-block temperatures at touchdown, were used in the computer simulation.

Body Block 1: C_B=5780 lb/ft²
Body Block 2: C_B=5480 lb/ft²
Body Block 3: C_B=5780 lb/ft²

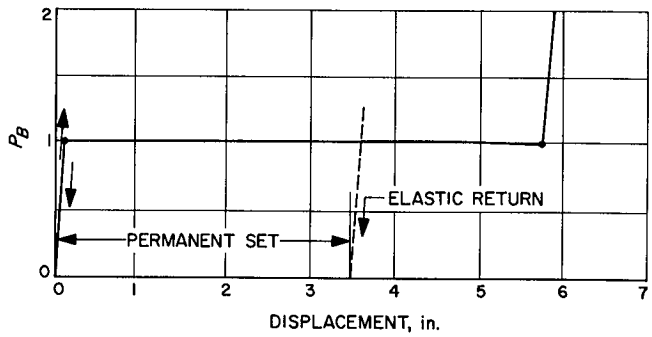

Fig. A-4. Typical block crush pressure profile

The profile P_B is shown in Fig. A-4. It is supplied to the computer in tabular form as shown in Table A-3.

Table A-3. Body-block characteristics

Displacement, in.	P_B
0	0
0.10	1.0
5.75	1.0
7.75	21.0

Linear interpolation is used between the listed values.

The profile P_B given above applies to each of the three body blocks.

References

1. Alderson, R. G., and Wells, D. A., *Final Report on Surveyor Lunar Touchdown Stability Study*, Report MM-66-19, Bendix Products Aerospace Division, South Bend, Indiana, July 8, 1966.
2. Deitrick, R. E., and Jones, R. H., *Touchdown Dynamics Study (Preliminary Report), Surveyor Spacecraft System*, Report SSD 3030R, Space Systems Division, Hughes Aircraft Company, Culver City, California, January 1963.
3. Garba, J. A., *A Comparison of Some Predicted and Measured Variables for a Full-Scale Surveyor Drop Test*, Technical Report 32-1084, Jet Propulsion Laboratory, Pasadena, Calif., March 1, 1967.

References (contd)

4. Harter, R. J., and Switz, R. J., "Analytical and Experimental Techniques Used to Establish Structural Design Loads for the Surveyor Spacecraft During Lunar Landing," *Shock and Vibration Bulletin No. 35*, Naval Research Laboratory, Washington, D. C., January 1966.
5. Rindfleisch, T., "Photometric Method for Lunar Topography," *Photogrammetric Engineering*, March 1966.
6. Jaffe, L. D., *Surveyor Project Lunar Scientific Model*, Project Document 54, Jet Propulsion Laboratory, Pasadena, Calif., April 1, 1966.
7. Christensen, E. M., et al., "Lunar Surface Mechanical Properties—Surveyor I," *Journal of Geophysical Research*, Vol. 72, No. 2, January 15, 1967.